# First $\beta$-Delayed Two-Neutron Spectroscopy of the $r$-Process Nucleus $^{134}$In and Observation of the $i_{13/2}$ Single-Particle Neutron State in $^{133}$Sn

P. Dyszel,[1] R. Grzywacz,[1] Z. Y. Xu,[1] N. Kitamura,[2] M. Karny,[3] A. Korgul,[3] M. Madurga,[1] S. Neupane,[4] A. Algora,[5] A. N. Andreyev,[6] M. Araszkiewicz,[3,7] R. A. Bark,[8] J. Benito,[9] N. Bernier,[9] M. J. G. Borge,[10] M. Caballero,[9] P. Chuchala,[3] T. E. Cocolios,[11] C. Costache,[12] J. G. Cubiss,[6,13] H. DeWitte,[11] J. E. Escher,[4] D. Fernandez-Ruiz,[10] A. Fijalkowska,[3] L. M. Fraile,[9] H. O. U. Fynbo,[14] J. Gouge,[1] J. L. Herraiz,[9] A. Illana,[9] P. M. Jones,[8] D. S. Judson,[15] P. Kamińska,[3] T. Kawano,[16] K. Kolos,[4] M. Labiche,[17] R. Lică,[18] M. Llanos-Expósito,[9] G. G. DeLorenzo,[9] N. Marginean,[12] I. Michelon,[19] C. Mihai,[18] E. Nácher,[20] C. Neacsu,[18] J. S. Nielsen,[14] B. Olaizola,[10] J. N. Orce,[21] C. A. A. Page,[6] R. D. Page,[15] J. Pakarinen,[22,23] A. Perea,[10] M. Piersa-Siłkowska,[1,9,24] Zs. Podolyák,[25] J. S. Prieto,[10] M. Rajabali,[26] J. Shaw,[11] A. I. Sison,[9] K. Solak,[3] M. Stryjczyk,[27,22] O. Tengblad,[10] P. G. T. Vicente,[9] N. Warr,[28] J. Wilson,[29] Z. Yue,[29] and S. Zajda[3]

(IDS Collaboration)

[1]*Department of Physics and Astronomy, University of Tennessee, Knoxville, Tennessee 37996, USA*
[2]*Center for Nuclear Study, University of Tokyo, Wako, Saitama 351-0198, Japan*
[3]*Faculty of Physics, University of Warsaw, PL 02-093 Warsaw, Poland*
[4]*Nuclear and Chemical Sciences Division, Lawrence Livermore National Laboratory, Livermore, California 94551, USA*
[5]*Instituto de Física Corpuscular, CSIC-Universidad de Valencia, E-46071, Valencia, Spain*
[6]*School of Physics, Engineering and Technology, University of York, York YO10 5DD, North Yorkshire, United Kingdom*
[7]*National Centre for Nuclear Research, Andrzeja SoÅ tana 7, 05-400 Otwock, Poland*
[8]*iThemba LABS, National Research Foundation, P.O. Box 722, Somerset West 7129, South Africa*
[9]*Grupo de Física Nuclear and IPARCOS, Universidad Complutense de Madrid, CEI Moncloa, E-28040 Madrid, Spain*
[10]*Instituto de Estructura de la Materia, CSIC, 28006 Madrid, Spain*
[11]*KU Leuven, Instituut, B-3001, Leuven, Belgium*
[12]*Horia Hulubei National Institute for Physics and Nuclear Engineering, RO-077125 Bucharest, Romania*
[13]*School of Physics and Astronomy, University of Edinburgh, Edinburgh, EH9 3FD, United Kingdom*
[14]*Department of Physics and Astronomy, Aarhus University, DK-8000 Aarhus C, Denmark*
[15]*Oliver Lodge Laboratory, University of Liverpool, Liverpool, L69 7ZE, United Kingdom*
[16]*Theoretical Division, Los Alamos National Lab, Los Alamos, New Mexico 87545, USA*
[17]*STFC Daresbury Laboratory, Daresbury, WA4 4AD, Warrington, United Kingdom*
[18]*Horia Hulubei National Institute of Physics and Nuclear Engineering (IFIN-HH), R-077125, Bucharest, Romania*
[19]*ISOLDE, EP Department, CERN, CH-1211 Geneva, Switzerland*
[20]*Instituto de Fisica Corpuscular, CSIC-Universidad de Valencia, E-46071 Valencia, Spain*
[21]*Department of Physics, University of the Western Cape, P/B X17 Bellville 7535, South Africa*
[22]*University of Jyväskylä, Department of Physics, P.O. Box 35, FI-40014, Jyväskylä, Finland*
[23]*Helsinki Institute of Physics, University of Helsinki, P.O. Box 64, FIN-00014 Helsinki, Finland*
[24]*Institute of Experimental Physics, Warsaw University, Warszawa, PL 00-681, Poland*
[25]*Department of Physics, University of Surrey, Guildford GU2 7XH, United Kingdom*
[26]*Department of Physics, Tennessee Technological University, Cookeville, TN 38505, USA*
[27]*Institut Laue-Langevin, 71 Avenue des Martyrs, F-38042 Grenoble, France*
[28]*Institut für Kernphysik, Universität zu Köln, 50937 Köln, Germany*
[29]*School of Physics, Engineering and Technology, University of York, York, YO10 5DD, United Kingdom*

(Received 20 March 2025; accepted 12 July 2025; published 8 October 2025)

This manuscript reports on the direct observation of a $\beta$-delayed two-neutron emission in a study of $^{134}$In at the ISOLDE Decay Station using neutron spectroscopy. We also report on the first measurement in $\beta^-$ decay of the long-sought $13/2^+$ excited state in $^{133}$Sn, attributed to be the neutron single-particle $i_{13/2}$

orbital. The observation of sequential neutron emission is used to extract the relative population of the $i_{13/2}$ state, which was found to be much smaller than the predictions of the statistical model. The experiment was possible because of the innovative use of a neutron array with neutron discrimination and interaction tracking capabilities. This is the first study of the details of the two-neutron emission for a nucleus, which belongs to the *r*-process path. Understanding $\beta$-delayed two-neutron emission probabilities is essential to validate models used in astrophysical *r*-process nucleosynthesis calculations. Observing two-neutron emissions in $\beta^-$ decay paves the way for new experiments to study energy and angular correlations for $\beta$-delayed multineutron emitters.

DOI: 10.1103/l24v-5m31

*Introduction*—$\beta$-delayed neutron emission ($\beta n$) is a common decay channel for most nuclei southeast of the valley of stability in the chart of nuclides. The process is possible when the $\beta$-decay energy window of the parent, $Q_{\beta^-}$, surpasses the neutron separation energy of the respective daughter, $S_{1n}$. In very neutron-rich nuclei, the dissimilarity between $Q_{\beta^-}$ and $S_{xn}(x \geq 2)$ energies opens the door for multineutron emission as an accessible decay mode. Experimental data on $\beta$-delayed neutron emitters are needed to validate models for nucleosynthesis in the *r* process [1]. This Letter presents the first $\beta$-delayed two-neutron ($\beta 2n$) spectroscopy of an *r*-process nucleus, $^{134}$In ($Z = 49, N = 85$), enabling a direct comparison between the experimental and model predicted branching ratios for the two-neutron emission process.

Experiments on $\beta$-delayed two-neutron emitters [2] are challenging due to the low production rates of $\beta 2n$ precursors, with nonnegligible $P_{2n}$, and difficulties in efficient and simultaneous detection of neutrons and their energies. For a broad range of *r*-process models, the predicted nucleosynthesis path involves directly $\beta$-delayed multineutron emitters ($\beta xn$) [1,3], which motivated programs of branching-ratio measurements [4–6]. The study of $\beta 2n$ precursors is a stepping stone toward understanding $\beta$-delayed multineutron emission.

Most of the nuclei on the *r*-process path are difficult or impossible to study experimentally, and astrophysical calculations heavily lean on nuclear models, which need experimental validation. In our previous work [7,8], we emphasized the need to reassess the basic assumptions underlying $\beta$-delayed neutron emission modeling. Predictions made by more comprehensive models may significantly impact the *r*-process freeze-out pattern caused by $\beta xn$ decay.

Currently, models used in astrophysics rely on the predictions given by the Hauser-Feshbach formalism [9], which assumes particles are emitted from structureless, compound nuclei [10]. In this framework, neutron emission probabilities depend only on spins, parities, and energies of the initial and final states. The neutron transmission coefficients are obtained using optical potentials. We have shown in our previous publications [7,8] that this approach may not be universally valid, especially in nuclei close to the shell closures, where the density of states is low, and the Bohr phenomenology of the compound nucleus may not be applicable in $\beta^-$ decay [11].

In nucleosynthesis, the region southeast of $^{132}$Sn in the chart of nuclides is of particular interest, as the $N = 82$ shell closure provides a persistent *r*-process trajectory governing the *r*-matter flow. Mumpower *et al.* concluded that nuclei in this region contribute greatly to the pattern of final elemental abundances [1]. Specifically, $^{134}$In can decay via $\beta 2n$ emission, making it an excellent candidate for studying energy correlation in two-neutron emission. This isotope has a large $\beta$-decay energy window ($Q_{\beta^-} = 14.46(20)$ MeV [12]), and the resulting $^{134}$Sn daughter has low one- and two-neutron separation energies at 3.631(4) and 6.030(4) MeV, respectively [12]. The $\beta^-$ decay is dominated by the $\nu g_{7/2} \rightarrow \pi g_{9/2}$ allowed Gamow-Teller (GT) transition, with minor contributions from first-forbidden transitions [13–15]. The dominant GT transition populates states around 7 MeV excitation energy in $^{134}$Sn [7] and is similar to particle-hole excitations observed in the $\beta^-$ decay of $^{133}$In [14,16]. Thus, it is an excellent candidate to study $\beta n$ and $\beta 2n$ decay. The reported probabilities are approximately 90% and 10%, respectively [6,15].

Additionally, the $\beta n$ decay of $^{134}$In is an efficient probe to observe neutron single-particle (s.p.) states in $^{133}$Sn that are not favored by the $\beta^-$ decay of $^{133}$In. Examples are the states at 854, 1561, and 2004 keV, which are attributed to a neutron outside the $^{132}$Sn core occupying the $p_{3/2}$, $h_{9/2}$, and $f_{5/2}$ orbitals, respectively [17,18]. These states are weakly populated in the $\beta^-$ decay of $^{133}$In as the GT transitions preferentially feed highly excited neutron-hole states in $^{133}$Sn [19]. The current ground-state spin assignment of $^{134}$In ($J^\pi = 6^-, 7^-$) [6,15] suggests the $\beta n$ decay should populate high-spin states in $^{133}$Sn, such as the $i_{13/2}$ s.p. state that is expected to be neutron-unbound [20,21]. The search for this state has been well underway for the last two decades [15,20–24]. An upper limit of 3.1 MeV was predicted for the excitation energy of this orbital [20,21]. Utilization of the NEXT detector (see the Appendix) allows for the unique capability to efficiently perform energy correlations between neutrons and reveal intermediate

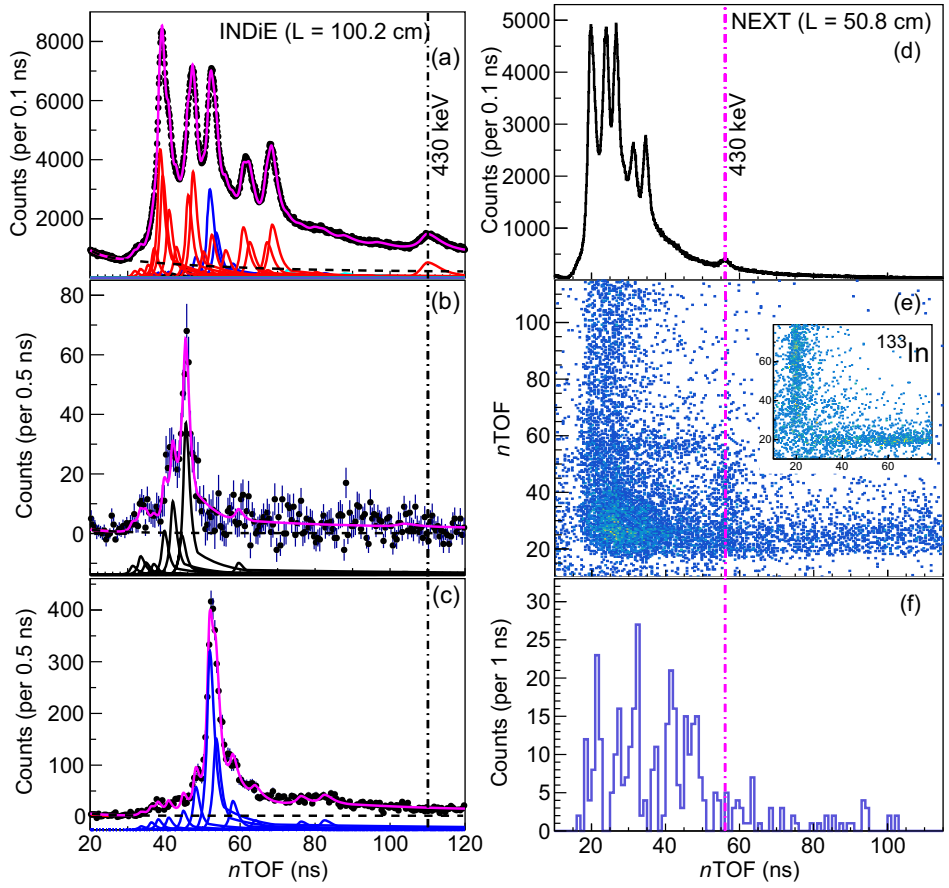


FIG. 1. Neutron TOF spectra in coincidence with $^{134}$In $\beta^-$ decay. Panels (a)–(c) show the neutron TOF spectra from INDiE, with neutron emission feeding the $^{133}$Sn ground-, first-, and second-excited states shown in red, black, and blue, respectively. The spectra were obtained by requiring coincidence with the $^{134}$In $\beta^-$ decay, with the 854-keV $\gamma$ ray ($3/2^- \rightarrow 7/2^-$ in $^{133}$Sn), and with the 1561-keV $\gamma$ ray ($9/2^- \rightarrow 7/2^-$ in $^{133}$Sn), respectively. The spectrum for neutrons in coincidence with fourth-excited state at 2004-keV is omitted from the figure due to weak feeding. The spectra were fit with the neutron response function (solid magenta) [14]. Panel (d) shows the PSD-gated neutron singles TOF spectrum from NEXT. Panel (e) shows coincident PSD-gated neutron events measured in NEXT, with the inset showing the same spectrum for $\beta$-delayed neutrons from $^{133}$In decay. Rejection criteria were applied to maximally suppress pure scattering events in $^{133}$In decay, which were then applied in the $^{134}$In analysis. Panel (f) shows the background subtracted neutron TOF spectrum in coincidence with 430(7) keV neutrons in $^{133}$Sn (see text), marked by the dashed magenta line in panels (d)–(f) at ≈56 ns.

states in $^{133}$Sn, including the long-sought $i_{13/2}$. So far the only potential evidence of successful two-neutron energy measurement in $\beta^-$ decay was reported for $^{11}$Li [25].

This Letter investigates the two-neutron emission events from the highly excited states in $^{134}$Sn populated in the $^{134}$In $\beta^-$ decay. We perform the first $\beta 2n$ spectroscopy of $^{134}$In and determine $\beta n$ feeding to the neutron-unbound $13/2^+$ state in $^{133}$Sn, which is a neutron $i_{13/2}$ s.p. state. Using a precisely calibrated neutron time-of-flight (nTOF) spectrometer, we established the excitation energy of the $13/2^+$ state.

*Experiment and results*—The experimental detection setup utilized HPGe clover detectors and two types of neutron detectors: the IDS Neutron Detector (INDiE) and the Neutron dEtector with Multi-neutron (Xn) Tracking (NEXT). A summary of the detection setup can be found in the Appendix.

The analysis of the nTOF spectrum utilized the known neutron response function from INDiE [14] in parallel with two-neutron emission events determined in NEXT. Figures 1(a)–1(c) show the nTOF spectra from INDiE with neutron emission feeding the $^{133}$Sn ground-, first-, and second-excited states in $^{133}$Sn (shown in red, black, and blue, respectively). The nTOF spectra were deconvoluted using $\chi^2$ fitting analysis and included five states in $^{133}$Sn; four neutron bound at 0-, 854-, 1561-, and 2004-keV ($J^\pi = 7/2^-, 3/2^-, 9/2^-$, and $5/2^-$, respectively, as shown in Fig. 2), and one neutron unbound. The nTOF deconvolution related to the feedings to neutron-bound states in $^{133}$Sn is outlined in Ref. [14], and that to a neutron-unbound state will be discussed hereafter.

To include $\beta 2n$ decays in the analysis, the NEXT detector was used to determine coincident two-neutron events as the PSD capability allows for a cleaner nTOF

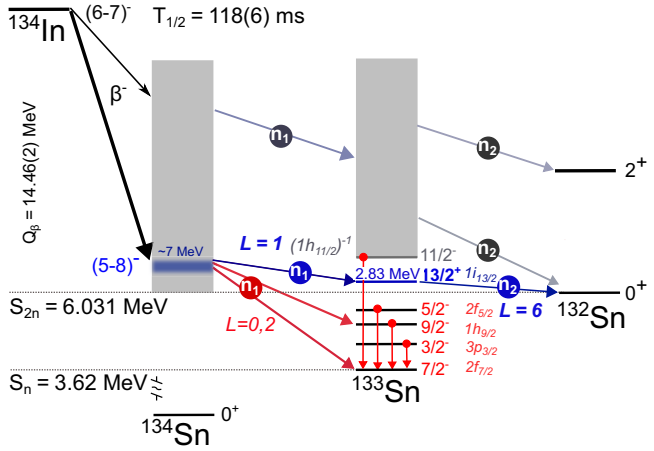


FIG. 2. Schematic decay scheme of $^{134}$In emphasizing $\beta n$ feeding to the $i_{13/2}$ s.p. orbital in $^{133}$Sn. The GT transitions from $^{134}$In strongly populate ~7 MeV excitations in $^{134}$Sn [7]. First neutrons ($n_1$) emitted from these excitations populate bound- and unbound-neutron states in $^{133}$Sn. The highlighted $n_1$ emission feeds the $i_{13/2}$ neutron state between the known $2f_{5/2}$ s.p. state and the $1h_{11/2}$ neutron-hole state in $^{133}$Sn. This state decays exclusively to the $^{132}$Sn ground state through second-neutron ($n_2$) emission; see text.

spectrum. Figures 1(d)–1(f) are the resulting TOF spectra following a PSD gate on neutron events measured with NEXT. Panel (d) shows the nTOF singles spectrum measured in the $^{134}$In $\beta^-$ decay. Panel (e) shows the two-neutron correlation matrices from $^{134}$In and $^{133}$In (shown in the inset) decays. A striking feature of this plot are the vertical and horizontal bands that indicate that there are neutrons emitted from $^{134}$Sn with a fixed energy in coincidence with neutrons emitted at varied energies. The inset shows regions of pure scattering as $^{133}$In has a negligible $\beta 2n$ channel [6]. Therefore, the existence of these bands following $^{134}$In decay corresponds to two-neutron emission. This plot can be interpreted in two separate scenarios depending on whether it is the first (from $^{134}$Sn) or the second neutron (from $^{133}$Sn) that has a fixed energy. The prior scenario can be rejected based on the nature of nuclear $\beta^-$ decay and the excited states in $^{133}$Sn and $^{132}$Sn; if the first neutron has a fixed energy, a particular $^{133}$Sn state is populated. It can only emit neutrons with varied energies if a series of low-lying excitations are available in $^{132}$Sn. Because of the doubly magic nature of $^{132}$Sn, the first excited state in this nucleus is high (4 MeV) and is populated very weakly [15]. Thus, only the second scenario is possible as the $\beta^-$ decay of $^{134}$In selectively populates states in $^{134}$Sn, as does the neutron emission of $^{134}$Sn for states in $^{133}$Sn.

In Fig. 1, the dot-dashed magenta (black) line at 56 ns (110 ns) represents the second emitted neutron at 430(7) keV in NEXT (INDiE), which aligns with the slowest neutron peak in panels (d) and (a), respectively. The error on the neutron energy was established from the deconvolution of INDiE. Panel (f) shows the summed background subtracted projections from panel (e) around the 56-ns (430 keV) region in NEXT. The peaks represent first-neutron candidates from $^{134}$Sn in coincidence with a 430-keV neutron from $^{133}$Sn, with the exception of a peak below 20 ns which is likely from scattering events which could not be rejected.

With the second neutron emitted from $^{133}$Sn at $E_n = 430(7)$-keV, a neutron-unbound state was established at 2829(8) keV [using $S_n(^{133}\mathrm{Sn}) = 2399(3)$ keV [12]]. Since there is currently no established neutron response function for the NEXT detector, the first-neutron candidates from Fig. 1(f) were implemented in the deconvolution of the INDiE nTOF spectrum by placing them in coincidence with a 2829 keV neutron-unbound state in $^{133}$Sn. We obtained the $\beta$-feeding probabilities ($I_\beta$) and $\beta n$ branching ratios after deconvolution by following the procedure outlined in Ref. [8].

*Assignment of the $i_{13/2}$ s.p. state*—Based on the presently known level scheme of $^{133}$Sn [14] and the fact that all other neutron s.p. states between the $N = 82$ and $N = 126$ shell gap have been measured [14,18], we assign $J^\pi = 13/2^+$ to the 2829(8)-keV state, which corresponds to the neutron $1i_{13/2}$ orbital. The argument is that it resides in $^{133}$Sn above the neutron $2f_{5/2}$ s.p. state ($J^\pi = 5/2^-$) at 2004 keV and below the lowest neutron-hole $(h_{11/2})^{-1}$ state ($J^\pi = 11/2^-$) at 3563 keV. If the neutron emission was from a more deeply bound orbital, it would surpass the excitation energy of $11/2^-$ in $^{133}$Sn. If the neutron occupies orbitals above the $N = 126$ shell closure, it would have a kinetic energy in excess of 4.5 MeV [26]. Therefore, we can reject other assignments. The energy of the $13/2^+$ state is consistent with that measured in a (d,p) experiment [27]. The simplified $^{134}$In decay scheme in Fig. 2 shows the relative structure of the levels in $^{133}$Sn, as well as sequential first and second neutrons feeding the ground state of $^{132}$Sn. The figure highlights in bold strongly populated ~7 MeV excitations in $^{134}$Sn [7], which can further decay through one- or two-neutron emission.

The $\gamma$-ray spectrum was inspected to seek for electromagnetic (EM) deexcitation from the $13/2^+$ state. Figure 3 shows the $\beta$- and $n$-gated $\gamma$-ray spectra from $\beta$ triggers, INDiE, and NEXT. We did not observe any $\gamma$ rays between 2700 and 2900 keV in coincidence with detected neutrons, which is not consistent with the observed 2792(3) keV $\gamma$ line from a one-neutron transfer reaction on $^{132}$Sn [24]. The 2434-keV $\gamma$ line observed in a previous $^{134}$In decay measurement [15] was discarded as it was not in coincidence with neutrons, either. The vertical colored band in Fig. 3 denotes our measurement at 2829 keV with a $\pm 3\sigma$ uncertainty; any peaks in the INDiE and NEXT neutron-gated $\gamma$-ray spectrum (red and green, respectively) are within $5\sigma$ of background, and are thus discarded.

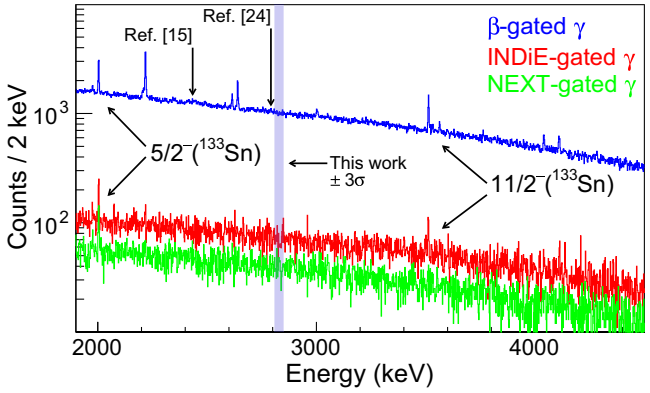


FIG. 3. $\beta$-gated $\gamma$-ray, and $n$-gated $\gamma$-ray spectra from INDiE and NEXT (blue, red, and green, respectively). Previous assignments for $i_{13/2}$ at 2434.2(3) keV [15] and 2792(3) keV [24] are shown along side the assignment from this work at $2829 \pm 3\sigma$ keV, denoted by the colored band. For reference, the 2005- and 3563-keV $\gamma$ lines ($5/2^-$ and $11/2^-$ states, respectively) in $^{133}$Sn are shown. EM deexcitations from the $i_{13/2}$ s.p. state were not observed.

The absence of $\gamma$ transition from the $13/2^+$ state to the $7/2^-$ ground state in $^{133}$Sn is consistent with the expectation of $E3$ transition probability, which is approximately five orders of magnitude weaker than neutron emission. The neutron width of the $13/2^+$ state was estimated using the WSPOT.FOR code [28] and the EM deexcitation probability was given by a generic Weisskopf estimate. No $\gamma-\gamma$ cascades depopulating the $13/2^+$ state were observed.

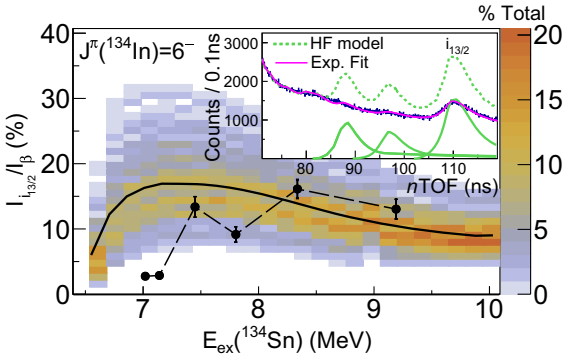


FIG. 4. Exclusive $\beta n$ branching ratio to the $i_{13/2}$ s.p. state in $^{133}$Sn as a function of populated excitations in $^{134}$Sn. $I_{i_{13/2}}/I_\beta$ is the relative branching between $i_{13/2}$ and the neutron-bound states in $^{133}$Sn obtained from the nTOF deconvolution. Experimental data points and errors are shown in black circles. The HF and KD-OMP calculations are averaged over the populated excitations in $^{134}$Sn from GT transitions; see text for details. The inset shows the late nTOF singles spectrum from Fig. 1(a). The solid magenta and dashed green lines represent the fit to experimental data and HF model predictions, respectively. The $i_{13/2}$ peak is labeled, while the peaks at ~88 and ~97 correspond to the ~7.15 and ~7.0 excitations in the main figure, respectively.

*Comparison with the Hauser-Feshbach model*—A highlight of our experimental finding is that from the nTOF deconvolution, we measured the $\beta n$ branchings to the $13/2^+$ state in $^{133}$Sn as a function of the $^{134}$Sn excitation energy. Figure 4 shows the comparison between experimental data and model predictions. Statistical model calculations using the Hauser-Feshbach (HF) formalism were performed using BeoH code [29,30]. The input requires knowledge of the spins, parities, and excitation energies of the initial and final states. Input data are taken from literature when possible [31]. Since $^{134}$In has a ground-state spin and parity of either $J^\pi = 6^-$ or $7^-$, we considered possible spin scenarios of the daughter nuclei for each ground state guided by selection rules through the GT transition ($\Delta J = 0, \pm 1$). Only results for $J^\pi(^{134}\mathrm{In}) = 6^-$ are shown as it was in better agreement with experimental data. The first-forbidden transitions populating positive-parity states were assumed to be extremely weak above 7 MeV [7,13,14].

In our analysis, we assessed the uncertainties related to the choice of the optical model parameters, which will affect relative neutron emission probabilities from excited states in $^{134}$Sn to states in $^{133}$Sn. We employed the Koning-Delaroche optical model potential (KD-OMP) [32] for nominal calculations of neutron transmission coefficients, and studied the sensitivity to variations of OMP parameters (outlined in Ref. [33]) in a similar manner as implemented in the study of potassium decays [8]. The calculation from the OMP and the comparison to experimental data are presented in Fig. 4, which shows the exclusive $\beta n$ branching ratio to the $i_{13/2}$ state as a function of excitation energy in $^{134}$Sn for $J^\pi(^{134}\mathrm{In}) = 6^-$. The multicolored band represents the density distribution of calculated neutron branching ratios, averaged over all possible GT transitions from the parent ground state, and includes all iterations of optical model parameters.

The results from the HF calculation are interpreted with simple qualitative arguments. Population of the $i_{13/2}$ state at 2829 keV in $^{133}$Sn is feasible at excitations above $3.63 + 2.83 \approx 6.5$ MeV in $^{134}$Sn. In the parity-conserving GT transitions, the $J^\pi = 5, 6, 7^-$ states in $^{134}$Sn are populated and $L = 1$ neutron emission to the $13/2^+$ state competes with higher energy $L = 2$ and $L = 4$ transitions to negative-parity bound states in $^{133}$Sn, [7]; see Fig. 2. The HF suggests that 200 keV above the available energy threshold, this population will exceed 5% for the considered range of OMPs.

For excitations in $^{134}$Sn near 7.5 MeV and above, experimental data are consistent with HF calculations indicating agreement with the statistical model in this region. A discrepancy occurs between the observed $\beta n$ branching and model predictions below 7.5 MeV, where feeding to $i_{13/2}$ from excitations at 7029- and 7143-keV in $^{134}$Sn is weaker by nearly a factor of six compared to the nominal calculation denoted by the black curve in Fig. 4.

The inset in Fig. 4 compares the experimental and model predicted nTOF spectra. The solid green peaks at ∼88 and ∼97 ns were scaled to match the predicted branching of Fig. 4, while the $i_{13/2}$ peak at ∼110 ns was scaled to reflect the peak amplitude required for such branching. This result indicates a strong hindrance of neutron emission to the $13/2^+$ state from excitations in $^{134}$Sn that are populated in the GT transitions compared to model predictions.

*Conclusions*—This Letter reports, for the first time, a detailed $\beta$-delayed two-neutron energy measurement for an $r$-process nucleus. The excitation energy of the long-sought $13/2^+$ state in $^{133}$Sn at 2829(8) keV was established, with no observed $\gamma$-ray branch. The precise determination of its excitation energy enabled a detailed comparison of the population of this state with HF predictions, which is used to model $\beta 2n$ decay probabilities. We found a significant hindrance of neutron emission from the strongly populated GT states in $^{134}$Sn to $13/2^+$ state in $^{133}$Sn. The origin of this hindrance cannot be explained by the uncertainties of OMPs, and could be attributed to a significant modification of nuclear potential or a violation of the compound nucleus assertion through our "doorway state" hypothesis [7,8], indicating a strong influence of nuclear structure effects on neutron emission. These results suggest that $r$-process models relying on HF models may not suffice to properly account for observed $\beta 2n$ branching. An exciting possibility to explain the hindrance could be the nonobservation of direct two-neutron emission which competes with hindered sequential emission. Unobserved EM transitions could also be depleting these excited states. Current analysis found no conclusive evidence for either in this high-statistics dataset. Our result of $\beta 2n$ decay paves the way for new experiments to study energy and angular correlations in $\beta xn$ emitters.

*Acknowledgments*—We acknowledge the support of the Isotope mass Separator OnLine facility (ISOLDE) Collaboration and technical teams. This project was supported by the European Union's HORIZON Programme under the Grant Agreement No. 101212216 (RADESO) and No. 101057511 (EUROLABS); the Office of Nuclear Physics, U.S. Department of Energy under Awards No. DE-FG02-96ER40983 (UTK) and No. DE-AC05-00OR22725 (ORNL); the auspices of the National Nuclear Security Administration of the U.S. Department of Energy at Los Alamos National Laboratory under Contract No. 89233218CNA000001; the U.S. Department of Energy at Lawrence Livermore National Laboratory under Contract No. DE-AC52-07NA27344; the National Nuclear Security Administration under the Stewardship Science Academic Alliances program through DOE Awards No. DE-436NA0003899, No. DE-NA0002132, and No. DE-NA0004068; the National Science Foundation through the Major Instrumentation Program Award No. 1919735; the Romanian IFA grant CERN/ISOLDE and Nucleus Project No. PN 23 21 01 02; the Research Foundation Flanders (FWO, Belgium) and the BOF KU Leuven (C14/22/104); the German BMBF under Contracts No. 05P18PKCIA and No. 05P21PKCI1 in Verbundprojekte 05P2018 and 05P2021; the UK Science and Technology Facilities Research Council (STFC) of the UK Grants No. ST/R004056/1, No. ST/P004598/1, No. ST/P003885/1, No. ST/V001027/1, ST/Y000242/1, and No. ST/V001035/1; the Guangdong Major Project of Basic and Applied Basic Research under Grant No. 2021B0301030006; the Polish National Science Center under Grants No. 2020/39/B/ST2/02346, No. 2024/53/N/ST2/03168, and No. 2023/51/D/ST2/02816; the Polish Ministry of Education and Science under Contract No. 2021/WK/07; the Spanish MCIN/AEI/10.13039/501100011033 under Grants No. PGC2018-093636-B-I00, No. RTI2018-098868-B-I00, No. PID2019–104390 GB-I00, No. PID2019–104714 GB-C21, No. PID2021-126998OB-I00, and No. PID2022-140162NB-I00; Generalitat Valenciana, Conselleria de Innovación, Universidades, Ciencia y Sociedad Digital under Grant No. CISEJI/2022/25; and the Universidad Complutense de Madrid (Spain) through Grupo de Física Nuclear (910059), J. B. also acknowledges support from a Complutense University of Madrid Margarita Salas CT31/21 Fellowship, funded by the Spanish MIU and European Union Next-Generation funds, RYC2021-031494-I. J. N. O., N. B., P. J., and R. B. acknowledge funding from the South African–CERN collaboration. The Hauser-Feshbach calculations were done using the BeoH code [29,30].

*Data availability*—The data are not publicly available. The data are available from the authors upon reasonable request.

[1] M. Mumpower, R. Surman, G. McLaughlin, and A. Aprahamian, Prog. Part. Nucl. Phys. **86**, 86 (2016).
[2] R. E. Azuma, L. C. Carraz, P. G. Hansen, B. Jonson, K. L. Kratz, S. Mattsson, G. Nyman, H. Ohm, H. L. Ravn, A. Schröder, and W. Ziegert, Phys. Rev. Lett. **43**, 1652 (1979).
[3] P. Möller, M. Mumpower, T. Kawano, and W. Myers, At. Data Nucl. Data Tables **125**, 1 (2019).
[4] K. Miernik, K. P. Rykaczewski, C. J. Gross, R. Grzywacz, M. Madurga, D. Miller, J. C. Batchelder, I. N. Borzov, N. T. Brewer, C. Jost, A. Korgul, C. Mazzocchi, A. J. Mendez, Y. Liu, S. V. Paulauskas, D. W. Stracener, J. A. Winger, M. Woli ńska Cichocka, and E. F. Zganjar, Phys. Rev. Lett. **111**, 132502 (2013).
[5] R. Yokoyama *et al.*, Phys. Rev. C **100**, 031302 (2019).
[6] V. H. Phong *et al.*, Phys. Rev. Lett. **129**, 172701 (2022).
[7] J. Heideman *et al.* (IDS Collaboration), Phys. Rev. C **108**, 024311 (2023).
[8] Z. Y. Xu *et al.*, Phys. Rev. Lett. **133**, 042501 (2024).
[9] W. Hauser and H. Feshbach, Phys. Rev. **87**, 366 (1952).
[10] T. Kawano, P. Möller, and W. B. Wilson, Phys. Rev. C **78**, 054601 (2008).

[11] N. Bohr and J. A. Wheeler, Phys. Rev. **56**, 426 (1939).
[12] M. Wang, W. Huang, F. Kondev, G. Audi, and S. Naimi, Chin. Phys. C **45**, 030003 (2021).
[13] I. N. Borzov, Phys. Rev. C **67**, 025802 (2003).
[14] Z. Y. Xu *et al.*, Phys. Rev. C **108**, 014314 (2023).
[15] M. Piersa-Siłkowska *et al.* (IDS Collaboration), Phys. Rev. C **104**, 044328 (2021).
[16] B. Fogelberg, M. Hellström, D. Jerrestam, H. Mach, J. Blomqvist, A. Kerek, L. O. Norlin, and J. P. Omtvedt, Phys. Rev. Lett. **73**, 2413 (1994).
[17] P. Hoff *et al.* (ISOLDE Collaboration), Phys. Rev. Lett. **77**, 1020 (1996).
[18] K. Jones *et al.*, Nature (London) **465**, 454 (2010).
[19] Z. Y. Xu *et al.*, Phys. Rev. Lett. **131**, 022501 (2023).
[20] W. Urban, W. Kurcewicz, A. Nowak, T. Rzaca-Urban, J. Durell, M. Leddy, M. Jones, W. Phillips, A. Smith, B. Varley, M. Bentaleb, E. Lubkiewicz, N. Schulz, J. Blomqvist, P. Daly, P. Bhattacharyya, C. Zhang, I. Ahmad, and L. Morss, Eur. Phys. J. A **5**, 239 (1999).
[21] Y. Lei and H. Jiang, Phys. Rev. C **90**, 047305 (2014).
[22] P. Hoff *et al.* (ISOLDE Collaboration), Hyperfine Interact. **129**, 141 (2000).
[23] A. Korgul, W. Urban, T. Rzaca-Urban, M. Rejmund, J. Durell, M. Leddy, M. Jones, W. Phillips, A. Smith, B. Varley, N. Schulz, M. Bentaleb, E. Lubkiewicz, I. Ahmad, and L. Morss, Eur. Phys. J. A **7**, 167 (2000).
[24] J. M. Allmond *et al.*, Phys. Rev. Lett. **112**, 172701 (2014).
[25] F. Delaunay *et al.*, Nuovo Cimento Soc. Ital. Fis. **42C**, 98 (2019).
[26] W. Long, P. Ring, J. Meng, N. Van Giai, and C. Bertulani, Phys. Rev. C **81**, 031302(R) (2010).
[27] B. Kay (private communication).
[28] B. A. Brown, WSPOT code, https://people.frib.msu.edu/~brown/reaction-codes/home.html.
[29] A. E. Lovell, T. Kawano, S. Okumura, I. Stetcu, M. R. Mumpower, and P. Talou, Phys. Rev. C **103**, 014615 (2021).
[30] S. Okumura, T. Kawano, P. T. Patrick Jaffke, and S. Chiba, J. Nucl. Sci. Technol. **55**, 1009 (2018).
[31] ENSDF database as of February 20th.
[32] A. Koning and J. Delaroche, Nucl. Phys. **A713**, 231 (2003).
[33] C. D. Pruitt, J. E. Escher, and R. Rahman, Phys. Rev. C **107**, 014602 (2023).
[34] R. Catherall, W. Andreazza, M. Breitenfeldt, A. Dorsival, G. J. Focker, T. P. Gharsa, G. T J, J.-L. Grenard, F. Locci, P. Martins, S. Marzari, J. Schipper, A. Shornikov, and T. Stora, J. Phys. G **44**, 094002 (2017).
[35] A. Gottberg, T. Mendonca, R. Luis, J. Ramos, C. Seiffert, S. Cimmino, S. Marzari, B. Crepieux, V. Manea, R. Wolf, F. Wienholtz, S. Kreim, V. Fedosseev, B. Marsh, S. Rothe, P. Vaz, J. Marques, and T. Stora, Nucl. Instrum. Methods Phys. Res., Sect. B **336**, 143 (2014).
[36] V. Fedosseev, K. Chrysalidis, T. D. Goodacre, B. Marsh, S. Rothe, C. Seiffert, and K. Wendt, J. Phys. G **44**, 084006 (2017).
[37] ISOLDE Collaboration, https://isolde-ids.web.cern.ch/.
[38] W. Peters *et al.*, Nucl. Instrum. Methods Phys. Res., Sect. A **836**, 122 (2016).
[39] S. Paulauskas, M. Madurga, R. Grzywacz, D. Miller, S. Padgett, and H. Tan, Nucl. Instrum. Methods Phys. Res., Sect. A **737**, 22 (2014).
[40] J. Heideman, D. Pérez-Loureiro, R. Grzywacz, C. Thornsberry, J. Chan, L. Heilbronn, S. Neupane, K. Schmitt, M. Rajabali, A. Engelhardt, C. Howell, L. Mostella, J. Owens, S. Shadrick, E. Peters, A. Ramirez, S. Yates, and K. Vaigneur, Nucl. Instrum. Methods Phys. Res., Sect. A **946**, 162528 (2019).
[41] S. Neupane, J. Heideman, R. Grzywacz, J. Hooker, K. Jones, N. Kitamura, C. Thornsberry, L. Heilbronn, M. Rajabali, Y. Alberty-Jones, J. Derkin, T. Massey, and D. Soltesz, Nucl. Instrum. Methods Phys. Res., Sect. A **1020**, 165881 (2021).
[42] S. Neupane, Development of a new high-resolution neutron detector and beta-delayed neutron spectroscopy of 24O, Ph.D. thesis, University of Tennessee, Knoxville, 2022.

## End Matter

*Appendix: Experimental setup*—The $^{134}$In beam was produced at the Isotope mass Separator On-Line (ISOLDE) facility at CERN [34]. A pulsed 1.4-GeV proton beam with an average current of 2 μA from the Proton Synchrotron Booster (PSB) impinged upon a solid tungsten proton-to-neutron converter [35] to produce spallation neutrons, used for neutron-induced fission in a nearby uranium-carbide target. Indium isotopes were ionized inside a hot cavity (maintained at ~2300 K to enhance diffusion and effusion) by the Resonance Ionization Laser Ion Source (RILIS) [36] in broadband mode to increase ionizing efficiency. The radioactive beam of $^{134}$In was separated via mass-to-charge ratio by the General Purpose Separator (GPS) and then transported to the ISOLDE Decay Station (IDS) where it was implanted onto a movable aluminized mylar tape [37] at the center of the decay chamber. The beam gate at ISOLDE was open for 530 ms following each proton pulse for continuous implantation. After the beam gate closed, the tape was immediately rolled into a shielded box to reduce contamination from subsequent daughter and granddaughter decays.

A schematic drawing of the experimental setup can be seen in Fig. 5. At IDS, four high-purity germanium (HPGe) clover detectors were placed 10 cm upstream from the implantation point to measure $\beta$-delayed $\gamma$ radiation. The energy deposition from Compton scattering inside all four crystals in each clover was summed to produce a $\gamma$-ray efficiency of 11% at 200 keV and 3.1% at 1 MeV. Three $\beta$

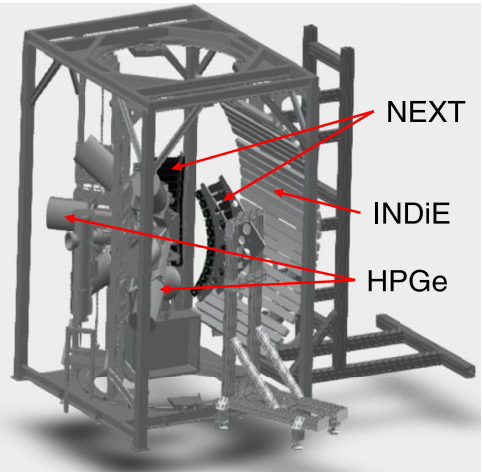


FIG. 5. Schematic drawing of the experimental setup at IDS. The $^{134}$In beam was implanted on the tape at the center of the setup. Four HPGe clover detectors upstream of the implantation point were used to detect $\beta$-delayed $\gamma$ rays. The INDiE and NEXT arrays were placed at 100.2 and 50.8 cm, respectively, from the implantation point for nTOF measurements.

triggers composed of EJ-204 plastic scintillator with dual-ended silicon photomultiplier (SiPM) readout surrounded the decay chamber and provided an average $\beta^-$ detection efficiency of ~80%. These $\beta$ triggers were used to deduce the start time of $\beta$-delayed neutron events. Neutron energies $E_n$ were determined by neutron TOF techniques for two different neutron detectors. The IDS Neutron Detector (INDiE), similar to the Versatile Array of Neutron Detectors at Low Energy (VANDLE) [38,39], consisted of 25 EJ-200 plastic scintillation modules fixed to an arch-shaped frame with a radius of 100 cm; see Fig. 1 in Ref. [14]. The flight path from the implantation point on the tape to the center of each module was found to be 100.2 cm by aligning the $^{133}$In $\beta n$ spectrum to previous data [14], covering a total solid angle of 12.2% of $4\pi$. The intrinsic neutron efficiency of each module is 55% at 1 MeV [38]. The traces of $\beta^-$ and neutron signals were sampled by 16-bit 250-MHz digitizers.

The Neutron dEtector with Multi-neutron (Xn) Tracking (NEXT) [40,41] array consisted of 28 modules fixed to two separate arch frames with a nominal 50-cm flight path. Each module is composed of an optically separated $4 \times 8$ segmented array of EJ-299 plastic scintillation material, which is capable of pulse-shape discrimination (PSD) between neutron and $\gamma$ events. Anger logic circuits allow for position readout [41] from position-sensitive photomultiplier tubes on each end of the detector. The actual flight path to the center of each module was determined to be 50.8 cm by aligning the $\beta n$ energy spectrum of $^{133}$In to the calibrated INDiE data. The solid-angle coverage was 10.6% of $4\pi$. The intrinsic neutron efficiency is 50% at 1 MeV [41]. Figure 5.4 in Ref. [42] shows an array of NEXT detectors, similar to those used in this measurement.